Practical Models for Practical Flexible Arms

Wayne Book
G.W.Woodruff School of Mechanical Engineering
Georgia Institute of Technology
Atlanta, GA 30332-0405

Klaus Obergfell
SeagateTechnology
7801 Computer Avenue South
Bloomington, MN 55435

Abstract

A laboratory robot with 3m links is modeled using an assumed mode method. The model is compared to experiments and to several theoretical limiting cases. The most demanding comparison is the comparison of frequency response results for joint motion, link deflection and tip deflection. We conclude that with care the models of an arm can be effective in controller design in spite of hydraulic actuators and non-ideal kinematics and structure.

Introduction

Flexible manipulator arms have been modeled for about 30 years [1,2] for the purpose of describing their dynamic behavior and improving it. Modeling is still very difficult to do in a practical and accurate way. Modeling techniques have advanced in sophistication over the years and nonlinear models with extensive consideration of the distributed parameter nature of the idealized mechanism can be constructed. In many cases the model needed for control design is much simpler and even linearized. However, if an arm with even reasonable complexity with practical design features and components comprises the physical system to be modeled, a detailed comparison between model and experiment is usually humbling.

This paper describes the recent modeling of a two-link manipulator arm named RALF (Robot Arm Large and Flexible). It is not the first time we have modeled this arm, but recent studies of tip position feedback necessitated a new look at the problem. The approach to the task and the results yielded are valuable to others modeling flexible motion systems. RALF is hydraulically actuated through a parallelogram mechanism presenting two complications that rarely appear in arm modeling papers. RALF's structure consists of a modest number of deviations from simple structural elements like straight beams. We present comparisons between this model, analytical models in limiting cases and experiments on the actual hardware.

Physical Description of RALF

The manipulator structure consists of two links and a parallel link mechanism for actuation of the upper link moving in a vertical plane. The two main links are 3.05 m (10 feet) long and constructed from round aluminum pipe while the lighter actuating link is rectangular in cross section. Thick sections of aluminum tubing connect the links to each other, to the actuators and to the base. The weights of the links without the sleeves are 12.18 kg (lower main), 8.8 kg (upper main), and 4.625 kg (actuating). The assembled manipulator structure without actuators and base weighs approximately 45 kg, while its payload capacity is approximately 27 kg.

Two single-rod hydraulic cylinders are used for actuation of RALF. A two-stage Moog hydraulic servo valve controls the fluid flow into each cylinder. Fluid is supplied at 1000 psi..

Linear position sensing transducers, which are attached to the hydraulic cylinders, measure cylinder length. A single, fixed vision sensor from DVT, Inc. referred to as a Landmark Tracking Sensor (LTS) measures the position of a landmark attached to RALF's tip in part of the manipulator's workspace as illustrated by the hatched area in Figure 1. When illuminated by a strobe a retro-reflective landmark is very bright resulting in a high contrast image. Additionally, the strobe freezes motion because of the very short flash duration. The computational resolution of the LTS is less than 0.4 mm in the horizontal direction and 0.5 mm in the vertical direction. Average speed of processing acquires images at about 50 Hz.

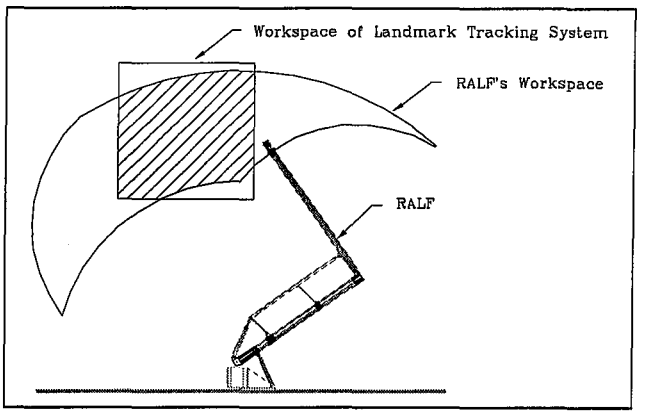

Figure 1: Schematic of RALF and its workspace.

A lateral effect photo-diode sensor and a lens, mounted to the inboard or proximal end of each link, is focused on a light source that is mounted to the outboard or distal end of the link. Measurements are made of the deflection of the link relative to the line of sight of the optics with a range of about +/- 30 mm within the accuracy of the 12 bit A/D converter.

Modeling

The purpose of the model developed here was to assist in selection and design of a joint actuator control that incorporated feedback of the tip position. One critical aspect of such a system is its non-minimum phase behavior. The ideal modeling procedure yields several models along the continuum from simple imprecise models to more complex and accurate models. It yields models that provide analytical forms for design procedures and numerical forms for simulation. Finally, a model should be verifiable in one or more ways and if the model does not match experiments on the physical system, the model should provide some means of improvement.

Dynamic Model of the Mechanism

A two-link flexible manipulator operating in the vertical plane is assumed. The link parameters (1) density, ρ, (2) cross-section area, A, (3) length, L, (4) modulus of elasticity, E, and (5) area moment of inertia, I, are assumed piece-wise constant. The manipulator is driven by two actuation torques. T_1 actuates the first link relative to the base, and T_2 actuates the second link relative to the first link. We will also assume that rotational speeds are small enough such that "centrifugal stiffening" is insignificant and that deformation amplitudes are small enough to ignore beam foreshortening.

The rigid body motion is described by the motion of a moving reference frame attached to the beam. The elastic deflection is described by a finite series of assumed modes with respect to the moving coordinate frame of the rigid body motion. The trial functions entered into the assumed modes method need only be admissible functions, i.e. satisfy the geometric boundary conditions which result from the choice of the rigid body coordinates. Two examples from previous work illustrate the choice of coordinates. Many researchers including Book [3] and Wang and Vidyasagar [4] aligned the rigid coordinate with the hub-angle and selected the modes of a clamped-free beam to describe the elastic motion. Kwon and Book [5] selected a rigid body coordinate that passes through the end-point of the link and the modes of a pinned-pinned beam. The hub-angle with clamped-free modes (HA/CF) approximates the system modes more closely, while the hub-to-tip with pinned-pinned modes (HT/PP) provides a simpler representation of the end-point position.

The HT/PP coordinates are illustrated in Figure 2 for a two-link arm. Note that the orientation of the second link is measured from a dashed line parallel to the x_1 axis and hence does not depend on the rotation at the end of the first link because the second link of RALF is actuated through a parallel link mechanism. This rotation would have to be considered if a motor mounted at the end of the first link actuated the second link. The same correspondence would be true for the HA/CF coordinates but is not shown here. This is consistent with the assumption that negligible foreshortening occurs in a bending beam.

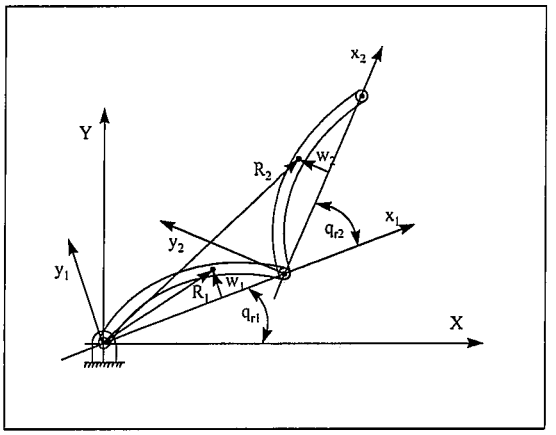

Figure 2: Model of RALF using HT/PP coordinates.

The position vectors for HA/CF coordinates are given in Obergfell [6] and are omitted here to save space. The position vectors for HT/PP coordinates shown in Figure 2 are given by:

$$R_1 = [x_1 Cosq_{r1} - w_1(x_1)Sinq_{r1}]i + [x_1 Sinq_{r1} + w_1(x_1)Cosq_{r1}]j \quad (1)$$

$$R_2 = [L_1 Cosq_{r1} + x_2 Cos(q_{r1}+q_{r2}) - w_2(x_2)Sin(q_{r1}+q_{r2})]i + [L_1 Sinq_{r1} + x_2 Sin(q_{r1}+q_{r2}) + w_2(x_2)Cos(q_{r1}+q_{r2})]j$$

For both coordinate systems, the elastic deflections are described by a finite sum of assumed modes:

$$w_i = \sum_{k=1}^{n} \psi_{ik}(x) q_{f,ik}(t) \quad (2)$$

q_f , ψ, and n are (time-dependent) flexible coordinates, (spatially-dependent) assumed modes, and number of modes per link, respectively. The total number of generalized coordinates of the two-link flexible manipulator is, therefore, given by $N = 2 + 2n$.

The natural modes of a clamped-free Bernoulli-Euler beam are used as the assumed modes for HA/CF coordinates. The natural modes of a pinned-pinned Bernoulli-Euler beam are used as the assumed modes for HT/PP coordinates. The k^{th} mode for the i^{th} link is given by:

$$\psi_{ik}(x_i) = \sin\frac{k\pi}{L_i} x_i \quad (3)$$

Note these assumed modes of a beam with a cross-section that changes over its length are no longer orthogonal.

The kinetic energy of the manipulator is obtained by integrating kinetic energy over the length of the links. For the i[th] link, this is given by

$$K_i = \frac{1}{2}\int_0^{L_i} \rho_i A_i < \dot{R}_i, \dot{R}_i > dx_i \tag{4}$$

where R_i is the position vector along link I, and $< >$ denotes an inner product.

The potential energy of RALF is stored as strain and gravitational potential energy. The strain potential energy of a beam in bending vibration is given by

$$P_{si} = \frac{1}{2}\int_0^{L_i} E_i I_i \left[\frac{\partial^2 w_i}{\partial x^2}\right]^2 dx_i \tag{5}$$

The gravitational potential energy in a field of strength g is obtained by integrating over the length of the links. For the i[th] link, this is given by

$$P_{gi} = g\int_0^{L_i} \rho_i A_i R_{yi} dx_i \tag{6}$$

where R_y is the vertical component of the position vector.

By substituting equations (1), (2), (3), (4), (5), and (6) for HT/PP coordinates or corresponding equations for HA/CF into Lagrange's equations, the equations of motion are obtained in matrix notation. They are given by the following:

$$[M(q)]\{\ddot{q}\} + \{C(q,\dot{q})\} + [K]\{q\} + \{G(q)\} = \{Q\} \tag{7}$$

$M(q)$, $C(q,\dot{q})$, K, and $G(q)$ are inertia matrix, coupling vector consisting of Coriolis and centrifugal terms, stiffness matrix, and vector of gravitational forces, respectively. The components of equation (7) are evaluated in symbolic form using Mathematica. Results are exported to Matlab/Simulink which is used for further processing including non-linear simulations.

Inputs and Outputs

When using HA/CF coordinates, the hub angles are identical to the rigid body coordinates, the link deflections are given by a linear relation of the flexible coordinates, and the end-point positions are given by a non-linear relation of rigid and flexible coordinates. When using HT/PP coordinates, the hub angle is given by a linear relation of rigid and flexible coordinates, the link deflection is given by a linear relation of flexible coordinates, and the end-point positions are given by a non-linear relation of rigid-body coordinates.

The system inputs enter the equations of motion through the generalized forces Q. The generalized forces are obtained from virtual work

$$\delta W = Q\delta q \tag{8}$$

where δq denotes a virtual displacement. The virtual work done by the torque T_k on the k[th] link of the manipulator is, therefore, given by

$$\delta W_k = T_k \delta\theta_k \tag{9}$$

where θ_k represents the angular displacement of the k[th] manipulator joint. The virtual displacement depends only on the rigid-body coordinates when HA/CF coordinates are used. However, when HT/PP-coordinates are used, the virtual displacement depends on rigid and flexible coordinates. The input influence matrix for HT/PP-coordinates is, therefore, given by

$$B_{HT/PP} = \begin{bmatrix} 1 & 0 & \frac{\partial \psi_{11}}{\partial x_1}(0) & \cdots & \frac{\partial \psi_{1n}}{\partial x_1}(0) & -\frac{\partial \psi_{11}}{\partial x_1}(0) & \cdots & -\frac{\partial \psi_{1n}}{\partial x_1}(0) \\ 0 & 1 & 0 & \cdots & 0 & \frac{\partial \psi_{21}}{\partial x_2}(0) & \cdots & \frac{\partial \psi_{2n}}{\partial x_2}(0) \end{bmatrix}^T \tag{10}$$

Linearization

Linearizing the non-linear manipulator dynamics is motivated by linear system identification methods applied in this work and by linear control methods envisioned for this manipulator and others often used. In addition, a study by Lee [7] has shown that the joint velocities achievable with the hydraulic actuators of RALF are too small to observe the velocity dependent non-linearities.

The linear manipulator dynamics are formally derived by expanding equation (7) in a Taylor series and ignoring higher order terms. This motivates the introduction of new coordinates which measure the deviation from the nominal operating point:

$$q - \overline{q} = \hat{q}, \dot{q} - \dot{\overline{q}} = \dot{\hat{q}}, \ddot{q} - \ddot{\overline{q}} = \ddot{q} - 0 = \ddot{\hat{q}}, T - \overline{T} = \hat{T} \tag{11}$$

In order to include empirical damping in the manipulator dynamics, the linear term $D\dot{q}$ is added to equation (7).

The dynamics are linearized at the stationary operating point,

$\dot{\overline{q}} = \ddot{\overline{q}} = 0$

and the effective inertia and stiffness matrices are decoupled using the modal matrix $[U]$:

$$m_{ii}] = [U]^T [M][U], [k_{ii}] = [U]^T [K][U] \tag{12}$$

yielding N decoupled equations. Given the measured damping ratio ζ_{exp}, the damping coefficients are obtained from the coefficients of equation (12):

$$d_i = 2\zeta_{exp,i}\sqrt{k_i m_i} \tag{13}$$

This yields a diagonal damping matrix which is transformed back to the original (coupled) coordinates by the inverse modal matrix:

$$D = [U]^{-T}[d_{ii}][U]^{-1} \tag{14}$$

Actuator dynamic models

Hydraulic servovalves contain an internal feedback mechanism to control the flow rate. At low frequencies this model would be equivalent to the velocity source model.

$$X_p(s) = \frac{1}{s}\left(C_1 E(s) - C_2 F_{ext}(s)\right) \tag{15}$$

Previous research by Lee [8] showed that the relative order between the terms inside the parentheses is 10^7 and equation (15) can, therefore, be simplified without significant loss of accuracy:

$$X_p(s) = \frac{1}{s}\frac{K_s K_a}{A_p} E(s) \tag{16}$$

F_{ext} the external force acting on the hydraulic cylinder piston

E the input voltage to the amplifier

K_a the amplifier gain (voltage-to-current)

K_s the servovalve gain

A_p the cross-sectional area of the hydraulic cylinder piston

X_p the linear displacement of the hydraulic cylinder piston

A block diagram combining structural model and proposed actuator model with proportional joint control is shown in Figure 3. The servovalves try to maintain a flow rate (joint velocity) that is proportional to the input voltage causing the hydraulic cylinders to apply a torque to RALF. The gain of the hydraulic actuators[1], $\hat{K}_{hydr}$, is determined from the frequency plots of RALF in Figure 4. The velocity feedback gain, K_v, will be determined such that the complete manipulator model matches the experimental results.

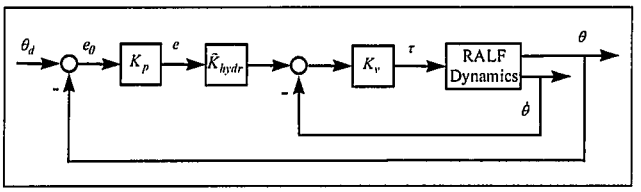

Figure 3: Block diagram of combined structure and actuator models with proportional joint control, actuator dynamics approximated by velocity feedback.

In order to better match experimentally determined link deflection and tip position response magnitudes the gain has to be raised to $K_{v1} = 45k$, $K_{v2} = 55k$. The natural frequencies of the resulting pole locations (4.8Hz and 7.4Hz) are slightly lower than for the velocity source model yet still higher than experimentally determined. However, given only one adjustment parameter, matching magnitudes of elastic responses was considered more important than an exact frequency match.

Verification

Given a model to be applied to a physical system, it is important that verification be made to minimize inappropriate modeling approximations, poor parameter values and outright errors in executing the model implementation. Below we have demonstrated some of the checks that can be made in making a comparison to other models and to experimental results.

Comparison to Single Link System Natural Frequencies

For initial verification, the natural frequencies of the models based on HA/CF and HT/PP coordinates are compared to theoretical predictions of natural frequencies for simple beams which are easily obtained from the literature, e.g. [9]. The model assumes that the links are uniform and includes three flexible modes per link (n=3). Increasing the modulus of elasticity of the first link by a factor of 20,000 transforms RALF into a pseudo-rigid/flex manipulator. With no control applied to the joints, the system exhibits two rigid body modes and a total of six flexible modes[2]. Because the joints are not restrained by control, the boundary conditions of the flexible link are pinned to the rigid link and free at the end-point. Results are given in Table 1.

The natural frequencies of the model with high-gain proportional-joint control are compared to those of a single beam with clamped-free boundary conditions. Results are given Table 2.

[1] $\hat{K}_{hydr}$ denotes the experimentally determined hydraulics gain relating voltage input to joint angle output while K_{hydr} denotes the actual hydraulic gain relating voltage input to cylinder velocity output.

[2] For this comparison, damping and gravity are turned off.

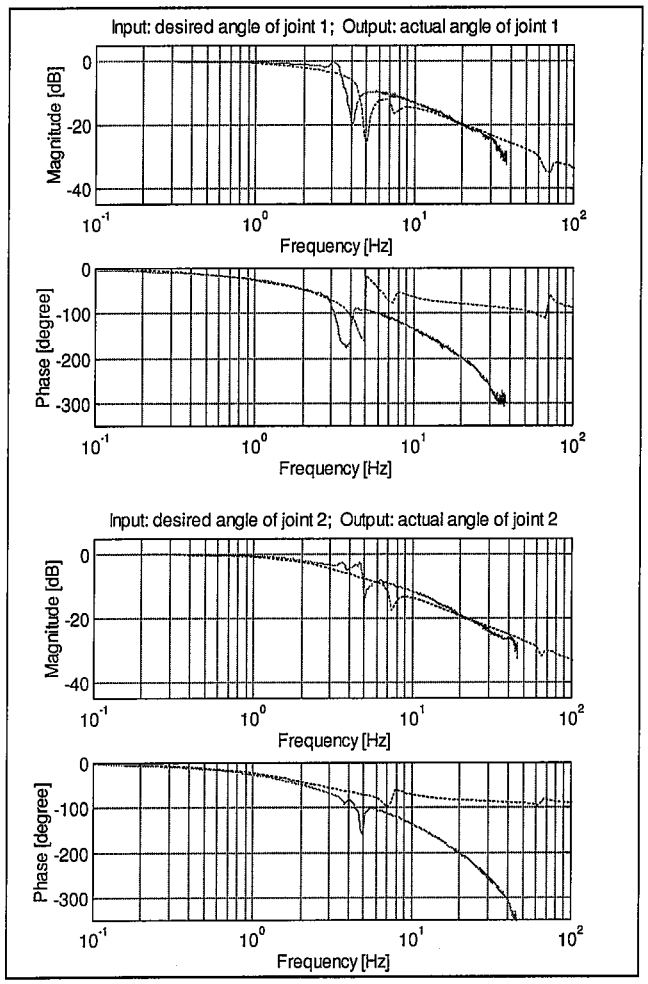

Figure 4: Frequency response of RALF's joints, experiment (solid) and model (dashed). Proportional joint control (K_{p1}=63k, K_{p2}=54k) is used to hold the manipulator at the operating point $(\theta_1 = 62.1°, \theta_2 = 81.1°)$.

Static Deflection Experiments

A static deflection experiment was performed to verify the stiffness of the RALF model with experimental data. Payloads were attached to the manipulator end-effector, and the relative deflection of the links was measured using the link deflection sensors on RALF. The experimental data was compared to the dynamic model and a static deflection model. The properties for RALF's main links are identical in both models; however, the static deflection model also includes the actuating link. Results are given in Table 3.

Measurements and model predictions compare well. Link 1 of the dynamic model is 15 % stiffer than RALF's first link. Link 2 of the dynamic model is 6 % more flexible than RALF's second link.

Reference beam	RALF-model HA/CF coordinates	RALF model HT/PP coordinates
52.91	52.50	2.51
171.47	170.53	0.67
357.76	553.74	6.28

Table 1: Natural frequencies of rigid/flex models and pinned-free reference beam (in Hz)

Reference beam	RALF-model HA/CF coordinates	RALF model HT/PP coordinates
12.07	11.96	13.62
75.63	74.94	87.53
211.76	209.82	277.68

Table 2: Natural frequencies (in Hz) of clamped-free reference beam and rigid/flex model with high-gain proportional joint control ($K_{p1}=10^{10}$, $K_{p2}=10^{10}$)

Natural Frequency Results without Actuators

In order to confirm the accuracy of the model's structural dynamics, a model was constructed which included only RALF's cross-sections and the weight of the actuation link. This model is comparable to RALF at the time of Huggins' experiments 10 The following is a comparison of this model to Huggins' experimental and theoretical findings as he investigated only structural dynamics without the inclusion of actuator dynamics. Results are given in Table 4.

Using either HA/CF or HT/PP coordinates, the models with two or three modes per link predict the first and second natural frequencies of RALF with a maximum error of 10%. The second natural frequency is actually more accurately predicted by the models using two or three modes than by Huggins' model. The third mode of RALF is dominated by the bending mode of the actuation link and is, therefore, not predicted by the serial-link model. The more complex fourth and fifth mode shapes are less accurately predicted by the serial-link model. The control of the first two modes of RALF are of most concern and the presented models predict these modes well.

Frequency Response Experiments

Huggins determined the natural frequencies and mode shapes of RALF at the home position. He excited the structure with an electro-mechanical shaker connected to the manipulator through a piezo-electric force transducer which measured the input signal. Magee [11] determined

	Experiment		Dynamic model		Static deflection model	
Payload (kg)	link 1 (mm)	link 2 (mm)	link 1 (mm)	link 2 (mm)	link 1 (mm)	link 2 (mm)
7.12	1.50	-2.75	1.43	-2.97	1.31	-2.89
14.22	3.20	-5.56	2.86	-5.94	2.62	-5.78
21.32	4.93	-8.42	4.29	-8.90	3.91	-8.67

Table 3: Static link deflection of RALF at home position. The dynamic model uses HT/PP coordinates with two modes per link.

	Huggins Experiment	Huggins Model	Model with HA/CF coordinates			Model with HT/PP coordinates		
No. Modes		2	3	2	1	3	2	1
1st bending mode of lower link	6.37	6.21	6.40	6.46	8.10	6.43	6.47	6.98
1st bending mode of upper link	12.00	16.90	13.05	13.21	15.18	13.21	13.24	14.65
1st bending mode of actuation link	37.87	30.76	-	-	-	-	-	-
2nd bending mode of lower link	57.37	95.40	74.13	84.47	-	77.02	81.92	-
2nd bending mode of upper link	94.02	98.25	80.46	87.30	-	84.87	91.62	-

Table 4: Comparison of RALF's natural frequencies (in Hz) at home position (ca. 1989 configuration). Constrained equations are utilized in Huggins' assumed modes model to include dynamic effects of the actuation link. Clamped-free boundary conditions of the other models are enforced using high-gain joint P-control ($K_{p1}=10^{10}$, $K_{p2}=10^{10}$).

the first natural frequency and damping ratio in RALF's whole workspace. A PD-joint control was applied to hold RALF at desired measurement locations. The structure was excited at the control level to include actuator dynamics by adding a random noise signal from the analyzer (the input signal) to the controller output. The system's response was measured by a tip-mounted accelerometer.

In this research, the structure excitation and data collection were programmed using the control computer, and frequency response was computed off-line using commercial software. A P-joint controller held RALF at the desired operating point. In order to investigate the effect of feedback on the system dynamics, experiments were repeated with high feedback gains (K_{p1}=63k, K_{p2}=54k) and low feedback gains (K_{p1}=28k, K_{p2}=24k).

Adding band-limited white noise or a swept sine to the nominal values of the joint controller excited the structure. The signal-to-noise ratio at high frequencies was low using noise excitation. However, the use of a swept sine allowed the investigation of separate frequency bands and the modification of input level as needed. In order to limit structural vibrations, the excitation amplitude was reduced in the frequency bands containing the fundamental frequencies. At higher frequencies, the excitation amplitude was increased to provide a sufficient signal-to-noise ratio. Using 10-12 overlapping frequency bands, the manipulator was excited from 0.01 Hz to 50 Hz. Two sweeps per frequency band were performed, one with increasing frequency and one with decreasing frequency.

The response of the structure was measured with all sensors available on RALF[3]. From this data, the frequency response was computed in the following three steps utilizing the Matlab Signal Processing Toolbox (1) the dc-values were removed from the individual data sets; (2) the individual time responses were combined into one long time response; and (3) the complex transfer function and coherence were computed using the "spectrum" function.

[3] For these experiments, the control, trajectory generation, and data gathering frequencies were set to 200 Hz . The sampling frequency of the LTS was set to 40 Hz.

The frequency response plots shown in this section were truncated after the coherence dropped to 0.4-0.6, which typically occurred at 35-45 Hz[4]. As the LTS was only sampled at 40 Hz, the corresponding frequency response was truncated at 13 Hz, 1/3 the sampling frequency.

The "open-loop"[5] frequency responses of joint 1 and joint 2 are similar to those of a simple integrator, i.e. amplitude drop of -20 dB/decade and a phase angle of -90° [6]. However, this approximation is not accurate near the resonance frequencies as evidenced by zeros in the magnitude at 4 Hz and 5 Hz for joints 1 and 2, respectively, independent of the feedback gain value used. As expected from the open-loop results, when feedback is applied, the outputs follow the inputs at low frequencies, as shown in Figure 4. At higher frequencies, the pole-zero-pole pattern exhibited in the open-loop plots is observed, and, therefore, the magnitude drops below 1. Also shown in Figure 4 are the experimental results which follow the model reasonably well except in terms of the phase angle. Additional phase shift can be due to time delays in the system that are not modeled.

Figure 6 shows the frequency response for deflection of link 2. Poles at 3.6, 5, and 30 Hz are observed for excitation by joints 1 and 2. The first two poles are more dominant than the third. When RALF is excited by joint 1, the first two poles have the same amplitude, and they are separated by a zero at 4.5 Hz. However, when RALF is excited by joint 2, the second pole is more dominant than the first, and the poles are separated by a zero at 4 Hz. Also shown are the corresponding model results.

The frequency response (model and experiment) for the tip position output (x direction) is shown in Figure 7 for excitation by joints 1 and 2. The first two natural frequencies at 3.6 and 5 Hz are clearly observed by the LTS. The third pole is not detected because it is located above the frequency range of the end-point position sensor.

In summary, experiments showed that the first three natural frequencies of RALF are located at 3.6, 5, and 30 Hz for the operating point of the manipulator. Huggins reported that the natural frequencies of RALF were located at 6.4, 12.0, and 37.9 Hz for the home position of the manipulator. It was anticipated that the natural frequencies would be lower than those reported by Huggins because of the modifications to the manipulator. Experimental plots follow the general shape of the model prediction but with errors in the exact placement of poles and zeros.

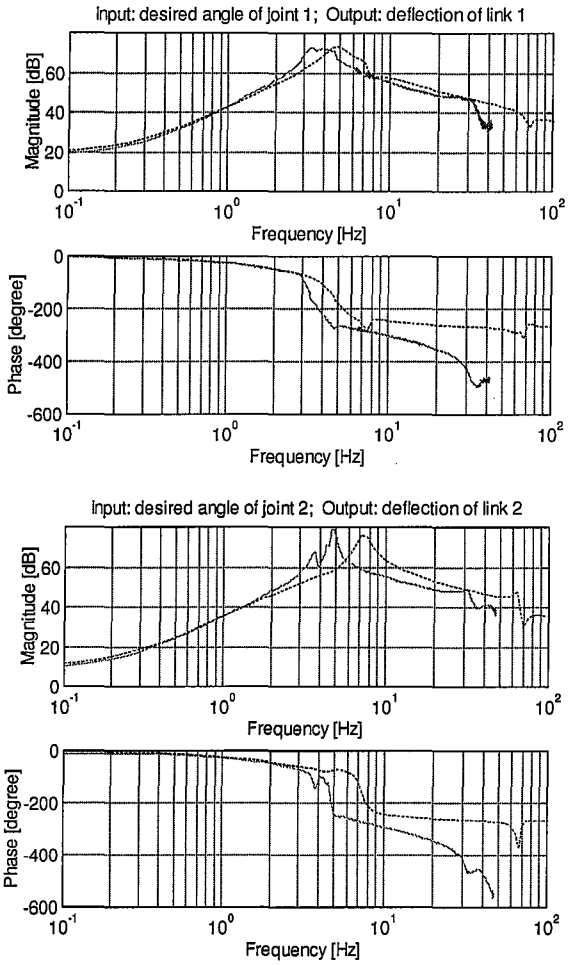

Figure 6: Frequency response of RALF's links, experiment (solid) and model (dashed). Proportional joint control is used to hold the manipulator at the operating point.

Discussion and Conclusion

RALF has structural and kinematic complexities such as offset attachments, variable link cross section and parallel links for actuation. In spite of the approximate manner for modeling these non-ideal characteristics, it is possible to get excellent agreement for natural frequencies with a relatively low order assumed modes model. For an actuated arm the hydraulic actuators must be included. Here it is important to recognize that hydraulic actuators are not torque sources but are reasonably well modeled by torque sources with velocity feedback. Additional accuracy in modeling the actuator would need to include the nonlinearities of the actuator, such as the nonsymmetrical behavior when the cylinders are extending and retracting due to the fact that the cylinder rod is found on one side of the piston, reducing the effective area of the piston on that side. We have compared the experimental frequency response to the frequency response of the model. The match is not

[4] The frequency response plots for joint 2 excitation are generally truncated at higher frequencies than the plots for joint 1 excitation because the identification procedure was improved during experimentation.

[5] P-joint control was used for all experiments. The term "open-loop" refers to transfer functions for the control signal input while closed-loop refers to transfer functions for the commanded joint angle input.

[6] Joint 2 is shifted by 180° because the direction of actuation and the hub angle are opposite.

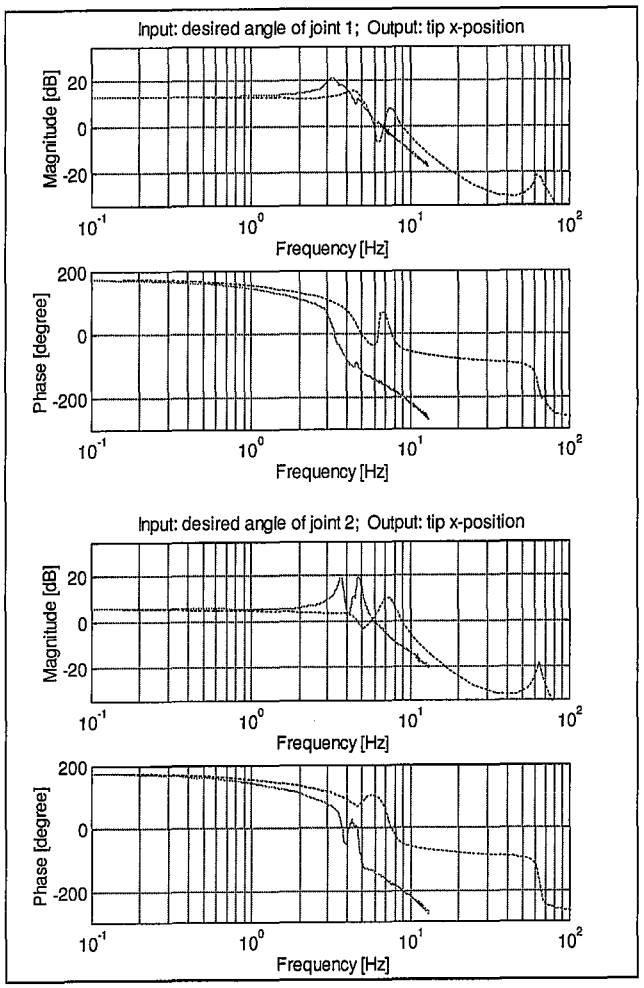

Figure 7: Frequency response of RALF's tip x-position, experiment (solid) and model (dashed). Proportional joint control is used to hold the manipulator at the operating point.

perfect, but represents reasonably well the qualitative and quantitative behavior. In some cases zeros of the system are not accurately predicted. This is noticeable in the case of the end point position measurement.

It is very valuable to be able to model and experiment in parallel. When the model and experiments disagree, it is often possible to track the problem to some omission in the model. Our model was probably not accurate enough to produce a final controller design, but it was close enough to evaluate a control strategy prior to a full implementation on a control computer and placing hardware at risk.

In conclusion, model expectations must be realistic, especially when nonlinear actuation schemes are to be employed. Modeling without verification against hardware is probably unreliable and any simulation of resulting behavior should be viewed as extremely preliminary.

1 Mirro, John, "Automatic Feedback Control of a Vibrating Flexible Beam," MS Thesis, Department of Mechanical Engineering, Massachusetts Institute of Technology, August, 1972.

2 Whitney, D.E., Book, W.J. and Lynch, P.M., "Design and Control Considerations for Industrial and Space Manipulators," Proceedings of the Joint Automatic Control Conference, June, 1974.

3 Book, W. J. ("Recursive Lagrangian Dynamics of Flexible Manipulator Arms", *International Journal of Robotics Research*, Vol. 3, No. 3, Fall 1984.

4 Wang, D. and Vidyasagar, M. "Transfer Functions for a Single Flexible Link", *The International Journal of Robotics Research*, Vol. 10, No. 5, October 1991, pp. 540-549.

5 Kwon, D.-S. and Book, W. J. "A Time-Domain Inverse Dynamic Tracking Control for a Single-Link Flexible Manipulator", *ASME Journal of Dynamic Systems, Measurement, and Control*, Vol. 116, No. 2, June 1994, pp. 193-200.

6 Obergfell, Klaus, End-Point Sensing and control of Flexible Multi-link Manipulators, Ph.D. Dissertation, Georgia Institute of Technology, August, 1998.

7 Lee, J. W. *Dynamic Analysis and Control of Lightweight Manipulators With Flexible Parallel Link Mechanisms*, Ph.D. Dissertation, Georgia Institute of Technology, June 1990.

8 Lee, S. H. *Robust Control of A Flexible Link Robot and Rigid Link Robot: Theory, Simulation, and Experiment*, Ph.D. Dissertation, Georgia Institute of Technology, March 1992.

9 Meirovitch, L. *Elements of Vibration Analysis*, 2 ed, 1986, McGraw-Hill.

10 Huggins, J. D., Experimental Verification of a Model of a Two-Link Flexible Manipulator, MS Thesis, Georgia Institute of Technology, June, 1988

11Magee, D. P. *Dynamic Control Modification Techniques in Teleoperation of a Flexible Manipulator*, M.S. Thesis, Georgia Institute of Technology, November 1991.